Elsevier Editorial System(tm) for Icarus
Manuscript Draft

Manuscript Number:

Title: Atomic oxygen on the Venus nightside: global distribution deduced from airglow mapping

Article Type: Regular Article

Keywords: Venus, atmosphere; Infrared observations; Atmospheres, composition

Corresponding Author: Miss Lauriane Soret,

Corresponding Author's Institution: Université de Liège

First Author: Lauriane Soret

Order of Authors: Lauriane Soret; Jean-Claude Gérard; Franck Montmessin; Giuseppe Piccioni; Pierre Drossart; Jean-Loup Bertaux

Abstract: The Visible and Infra-Red Thermal Imaging Spectrometer (VIRTIS) instrument on board the Venus Express spacecraft has measured the O2(a1Δ) nightglow distribution at 1.27 μm in the Venus mesosphere for more than two years. Nadir observations have been used to create a statistical map of the emission on Venus nightside. It appears that the statistical 1.6 MR maximum of the emission is located around the antisolar point. Limb observations provide information on the altitude and on the shape of the emission layer. We combine nadir observations essentially covering the southern hemisphere, corrected for the thermal emission of the lower atmosphere with limb profiles of the northern hemisphere to generate a global map of the Venus nightside emission at 1.27 μm. Given all the O2(a1Δ) intensity profiles, O2(a1Δ) and O density profiles have been calculated and three-dimensional maps of metastable molecular and atomic oxygen densities have been generated. The O2(a1Δ) hemispheric average density is 2.1x109 cm-3 at 99.2 km, with a maximum value of 6.5x109 cm-3. The O density profiles have been derived from the nightglow data using CO2 profiles from the empirical VTS3 model or from SPICAV stellar occultations. The O hemispheric average density is 1.9x1011 cm-3 in both cases, with a mean altitude of the peak located at 106.1 km and 103.4 km, respectively. This global O density nightside distribution improves that available from the VTS3 model, which was obtained by extrapolating measurements made above 145 km. Comparing the oxygen density map derived from the O2(a1Δ) nightglow observations, it appears that the morphology is very different and that the densities obtained in this study are about three times higher than those predicted by the VTS3 model.

Suggested Reviewers: Stephen Bougher
University of Michigan
bougher@umich.edu
Stephen Bougher works on the three-dimensional Venus Thermospheric General Circulation Model, which combines chemical, dynamical and energetic processes. Oxygen aiglow and density distributions are parameters he is especially taking into account.

Tom Slanger
SRI
tom.slanger@sri.com

Tom Slanger discovered the atomic oxygen green line in the Venus night airglow. He is a 40 year expert on oxygen recombination.

Jeremy Bailey
University of New South Wales
j.bailey@unsw.edu.au
Jeremy Bailey works on the Venus oxygen nightglow, using ground-based observations.

Opposed Reviewers:

Manuscript
Click here to view linked References

Atomic oxygen on the Venus nightside: global distribution deduced from airglow mapping

L. Soret[1]

J.-C. Gérard[1]

F. Montmessin[2]

G. Piccioni[3]

P. Drossart[4]

J.-L. Bertaux[2]

[1]Laboratoire de Physique Atmosphérique et Planétaire, Université de Liège, Belgium

[2]LATMOS, Guyancourt, France

[3]IASF-INAF, Roma, Italy

[4]Observatoire de Paris, Meudon, France

Abstract

The Visible and Infra-Red Thermal Imaging Spectrometer (VIRTIS) instrument on board the Venus Express spacecraft has measured the $O_2(a^1\Delta)$ nightglow distribution at 1.27 µm in the Venus mesosphere for more than two years. Nadir observations have been used to create a statistical map of the emission on Venus nightside. It appears that the statistical 1.6 MR maximum of the emission is located around the antisolar point. Limb observations provide information on the altitude and on the shape of the emission layer. We combine nadir observations essentially covering the southern hemisphere, corrected for the thermal emission of the lower atmosphere with limb profiles of the northern hemisphere to generate a global map of the Venus nightside emission at 1.27 µm. Given all the $O_2(a^1\Delta)$ intensity profiles, $O_2(a^1\Delta)$ and O density profiles have been calculated and three-dimensional maps of metastable molecular and atomic oxygen densities have been generated. The $O_2(a^1\Delta)$ hemispheric average density is $2.1x10^9$ cm^{-3} at 99.2 km, with a maximum value of $6.5x10^9$ cm^{-3}. The O density profiles have been derived from the nightglow data using CO_2 profiles from the empirical VTS3 model or from SPICAV stellar occultations. The O hemispheric average density is $1.9x10^{11}$ cm^{-3} in both cases, with a mean altitude of the peak located at 106.1 km and 103.4 km, respectively. This global O density nightside distribution improves that available from the VTS3 model, which was obtained by extrapolating measurements made above 145 km. Comparing the oxygen density map derived from the $O_2(a^1\Delta)$ nightglow observations, it appears that the morphology is very different and that the densities obtained in this study are about three times higher than those predicted by the VTS3 model.

1. Introduction

In situ mass spectrometer measurements have shown that atomic oxygen is a major constituent of the Venus nightside thermosphere between 140 and 170 km (Niemann *et al.*, 1980) but no in situ measurements have been made below 140 km. (Gérard *et al.*, 2009) showed that the atomic oxygen density can be deduced from the $O_2(a^1\Delta)$ volume emission rate. The $O_2(a^1\Delta)$ nightglow in the Venus upper mesosphere has been observed at 1.27 µm from the ground (Bailey *et al.*, 2008; Crisp *et al.*, 1996; Ohtsuki *et al.*, 2005; 2008) and using data from the Visible and Infra-Red Thermal Imaging Spectrometer (VIRTIS) instrument on board the Venus Express spacecraft (Drossart *et al.*, 2007; Piccioni *et al.*, 2009). The Venus Express orbiter was launched by the European Space Agency (ESA) on November 2005. Since April 2006, it has been orbiting around Venus in a 24-hour polar elliptical orbit. Its pericenter is located near 250 km while the altitude of its apocenter is 66 000 km. VIRTIS is composed of two spectrometers: the VIRTIS-M medium-spectral resolution imaging spectrometer and the VIRTIS-H high-spectral resolution spectrometer. VIRTIS-M can be used in the visible/NIR channel from 0.3 to 1 µm by steps of ~2 nm or in the IR channel from 1 to 5 µm by steps of ~10 nm. The VIRTIS-M-IR instrument is well adapted to the observation of the $O_2(a^1\Delta)$ nightglow at 1.27 µm either in nadir or limb modes. Using nadir observations, Gérard *et al.* (2008) and Piccioni *et al.* (2009) found that the emission peak was statistically located around the antisolar point, with a maximum value of respectively 3 MR and 1.2 MR (1 Rayleigh, R, corresponds to the brightness of an extended source emitting 10^6 photons cm^{-2} s^{-1} in 4π sr) and a mean intensity for Venus nightside of 1.3 MR and 0.52 MR, respectively. Using limb observations, the mean brightness at the maximum of the profile obtained along the line of sight was found to be 28±22 MR at 96±2.7 km by Gérard *et al.* (2010). Connes *et al.* (1979) suggested that the observed emission corresponds to radiative

deexcitation of the $O_2(a^1\Delta)$ molecules following three-body recombination of oxygen atoms. These atoms are produced on the Venus dayside by photodissociation and electron impact dissociation of CO_2 and CO and transported to the nightside by solar to antisolar (SSAS) circulation. The reaction scheme may be written:

$$2O + CO_2 \rightarrow O_2* + CO_2 \qquad (k) \qquad 1$$

$$O_2* \rightarrow O_2 + h\nu \qquad (A) \qquad 2$$

$$O_2* + CO_2 \rightarrow O_2 + CO_2 \qquad (C_q) \qquad 3$$

where O_2* represents excited oxygen molecules, k=3.1x10^{-32} cm^6 s^{-1} is the reaction rate coefficient of reaction (1), A=2.19x10^{-4} s^{-1} is the Einstein coefficient of the 1.27 µm transition and Cq is the quenching coefficient. Because this coefficient is very low, it has not been possible to determine its exact value. Sander *et al.* (2003) recommend using an upper limit value of 2x10^{-20} cm^{-3} s^{-1}. The k reaction rate is estimated to be 2.5 times the rate coefficient for oxygen atom three-body recombination in nitrogen taken to be 1.25x10^{-32} cm^6 s^{-1} (Huestis *et al.*, 2008; Slanger *et al.*, 2006) at 187 K, which is the rotational temperature estimated by Bailey *et al.* (2008) from best fits to ground-based observations with a forward modeling approach. Based on these reactions and VIRTIS-M-IR nadir and limb $O_2(a^1\Delta)$ observations, it is possible to deduce $O_2(a^1\Delta)$ density profiles between 90 and 120 km (Gérard *et al.*, 2009). Atomic oxygen density profiles can also be calculated if CO_2 density profiles are available (see reaction 3). The CO_2 density vertical distribution can be obtained using either results from the Venus International Reference atmosphere (VIRA) model or observations from Venus Express. The empirical VIRA model (Keating *et al.*, 1985) is largely based on

measurements performed above ~145 km by the Orbiting Neutral Mass Spectrometer (ONMS) on board the Pioneer Venus orbiter from 1978 to 1980 during a period of high solar activity. Below this altitude, the VTS3 numerical implementation empirical model by Hedin *et al.* (1983) extrapolates the O density profiles assuming hydrostatic equilibrium.

The Spectroscopy for the Investigation of the Characteristics of the Atmosphere of Venus (SPICAV) instrument is a suite of three spectrometers in the UV and IR range flying on the Venus Express orbiter (Bertaux *et al.,* 2007). The UV sensor, which covers the range extending from 118 to 320 nm, provides vertical profiles of CO_2 in the stellar occultation mode. For this study, we used 114 processed CO_2 profiles retrieved from SPICAV stellar occultation observations.

In section 2, we describe how limb and nadir observations from the VIRTIS instrument on board Venus Express have been combined to generate a three-dimensional map of the $O_2(a^1\Delta)$ emission in the mesosphere-thermosphere transition region on the Venus nightside. Section 3 explains how a three-dimensional map of the atomic oxygen density has been generated by combining results from section 2 and three-dimensional maps of the CO_2 density, using either results from the empirical VTS3 model or observational data from the SPICAV instrument.

2. Three-dimensional map of the $O_2(a^1\Delta)$ emission

Two types of observations can be used to observe Venus with VIRTIS: the limb and the nadir modes. Because of the spacecraft's polar elliptical orbit, nadir measurements are preferentially made while VIRTIS observes the southern hemisphere. Nadir observations measure the $O_2(a^1\Delta)$ emission brightness over wide ranges of latitudes and local times. Instead, limb observations are collected in the northern hemisphere. The coverage is more limited but the third dimension (the emission rate as a function of altitude) is also available.

The following paragraphs explain how both nadir and limb observations have been mixed together to generate a three-dimensional map of the $O_2(a^1\Delta)$ emission over the entire Venus nightside.

2.1. Generation of a two-dimensional map of the $O_2(a^1\Delta)$ emission using nadir and limb observations

Generating a global statistical map of the $O_2(a^1\Delta)$ emission requires to process nadir and limb data separately. Nadir observations showing the $O_2(a^1\Delta)$ emission also include a thermal contribution which first has to be removed. To do so, Cardesin-Moinelo 2009 recommends considering the bands 1.23 to 1.30 µm of a VIRTIS-M-IR observation for the airglow emission. A continuum contribution determined from the 1.23 and 1.30 µm channels is then subtracted from this emission. The thermal contribution originating from hot regions of the surface and lower atmosphere is estimated between 1.14 and 1.21 µm. A continuum is also subtracted by using the signal in the 1.14 and 1.21 µm channels. Thirty percents of this thermal band is then subtracted from the airglow emission band (Piccioni *et al.,* 2009). The data are corrected for emission angle and backscattering following the method developed by Crisp *et al.* (1996). Finally, all the images acquired by VIRTIS-M-IR are assembled to generate a global map of the nadir observations.

Profiles of the $O_2(a^1\Delta)$ emission as a function of altitude are extracted from limb observations. As limb observations can vary either in latitude or local time, profiles are extracted by range of 1° of the varying parameter (Gérard *et al.,* 2010). These profiles are then deconvolved to account for the spatial resolution of the instrument which is 15 km near apocenter at 66 000 km. The local volume emission rate is then deduced from these profiles by applying the inverse Abel transform (Gérard *et al.,* 2009):

$$\eta(z) = \frac{-1}{\pi} \int_{z}^{+\infty} \frac{dI}{dz_0} \frac{dz_0}{\sqrt{z_0^2 - z^2}} \qquad 4$$

where η is the local O_2 emission rate expressed in cm^{-3} s^{-1}, z is the distance from the center of Venus in km, I is the brightness along the line of sight expressed in photons cm^{-2} s^{-1}. These local volume emission rate profiles can then be vertically integrated along the altitude to simulate nadir observations. Finally, combining the map of nadir observations in the southern hemisphere and the one of vertically integrated limb observations from the northern hemisphere provides a statistical global map of the $O_2(a^1\Delta)$ emission. Figure 1-a shows the nadir intensities obtained with this method. This statistical map has been generated using from one observation for the pixels of the northern hemisphere to 360 observations for the pixels located at high southern latitudes. A region of enhanced emission appears around the antisolar point, with a maximum brightness of 1.6 MR. It is clearly observed that the intensity decreases away from the antisolar point. The morphology of this map is in good agreement with previous results from Gérard *et al.* (2008) and Piccioni *et al.* (2009) who obtained 3.0 MR and 1.2 MR for the maximum brightness of the $O_2(a^1\Delta)$ emission, respectively. We note that the thermal contribution was under-estimated by Gérard *et al.* (2008) and that the intensities showed in the map of Piccioni *et al.* (2009) were represented with a maximum level of 1.2 MR. The mean brightness on Venus nightside is I_m=0.50 MR, taking into account the actual area weight of each useable pixel (1 pixel is 1° of latitude by 1° of longitude). Assuming that the efficiency of O atoms recombining directly or by cascades from upper lying states into the $a^1\Delta$ state is ε=0.75 and that the only O loss on the nightside is reaction 1, the following relation is obtained:

$$I_m = 0.37 \times 10^{-12} . \Phi_O \qquad 5$$

where Φ_O is the downward flux of O atoms at 130 km (Gérard *et al.,* 2008). Thus, a mean hemispheric value of 0.50 MR corresponds to an average downward flux of Φ_O=1.35x10^{12} cm^{-2} s^{-1}, which is about 17% of the average production on the dayside estimated to range between 6.4x10^{12} cm^{-2} s^{-1} (Krasnopolsky, 2010) and 8x10^{12} cm^{-2} s^{-1} (Leu and Yung 1987). This implies that 17% to 22% of the dayside production of O atoms is transported to the nightside where they recombine and produce the $O_2(a^1\Delta)$ nightglow. If other processes involving destruction of O atoms through reactions with odd hydrogen and chlorine are considered, relation 5 no longer holds. In this case a larger downward flux of O is needed to produce a given vertical $O_2(a^1\Delta)$ emission rate. Krasnopolsky (2010) concluded that approximately 50% of the atomic oxygen is lost on the nightside through three-body recombination. In this case, the efficiency of the transfer from the day to the nightside is ~34 to 44%.

2.2. Generation of a new data set of $O_2(a^1\Delta)$ limb profiles

Next, we analyze limb observations to access the brightness of the emission along the atmospheric column. Limb profiles have been deduced from observations covering almost all the northern hemisphere and are extremely variable. Piccioni *et al.* (2009) showed that the peak altitude is located between 90 and 103 km with intensities along the line of sight ranging from 4 to 100 MR. Gérard *et al.* (2010) obtained a mean peak altitude of 96 ± 2.7 km and a mean intensity of 28 ± 23 MR. However, according to Figure 1-a, the intensity is brighter around the antisolar point and appears to decrease with the distance from this point. We thus decided to generate mean $O_2(a^1\Delta)$ limb profiles every 5° of solar zenith angle. Figure 2-a shows these averaged limb profiles, the red profiles being deduced from observations near the antisolar point and the blue ones near the terminator. It clearly appears that the peak intensity

along the line of sight decreases away from the antisolar point. The peak brightness is 66.3 MR at the antisolar point while it drops down to 6.7 MR near the terminator. As can be seen from Figure 2-a and confirmed in Figure 2-b, the peak altitude of the $O_2(a^1\Delta)$ emission statistically tends to increase from 94 to 99 km from the antisolar point to 80° of solar zenith angle. These results were obtained with observations collected in the northern hemisphere. In the absence of data for the southern hemisphere, we assume that the presence of a hemispheric symmetry and we use these profiles for the entire nightside. They will be referred to as *reference profiles*.

2.3. Combination of the global nadir map and the averaged limb profiles

At this point, we have constructed a global statistical map of nadir values (Figure 1-a) and statistical limb profiles of the $O_2(a^1\Delta)$ emission (Figure 2-a). Each point of the Venus nightside is characterized by its coordinates (latitude and local time). The nadir intensity of each point can be determined from the statistical map. A limb profile can also be associated with this specific point by normalizing the appropriate reference limb profile (given the solar zenith angle of this point) to the mapped nadir intensity. The method to normalize a reference profile is specified hereafter. First, the local emission rate is deduced from observations integrated along the line of sight by the inverse Abel transform (see equation 4). This local profile is then vertically integrated to obtain the intensity of a simulated nadir observation. This value is then compared to the actual nadir intensity retrieved from the statistical map. Using this ratio, the vertical emission rate profile can be normalized. Finally, the normalized limb profile is calculated by applying the Abel transform to this local profile. As this process can be applied to every single point of the Venus nightside, we finally obtain a three-dimensional map of the $O_2(a^1\Delta)$ emission. As an example, Figure 1-b shows a cross section at

a given altitude (here 96.5 km) of the $O_2(a^1\Delta)$ intensity along the line of sight. As the peak emission is located near 96.5 km (Gérard *et al.*, 2008; 2010; Piccioni *et al.*, 2009) and as the normalization has been made using the nadir values of the statistical map, it is natural that Figure 1-b shows the same morphology as Figure 1-a.

3. Three-dimensional map of atomic oxygen density

Now that every pixel of the Venus nightside is associated to a limb profile, $O_2(a^1\Delta)$ densities can be deduced. Using these and CO_2 densities, it is possible to generate vertical profiles of atomic oxygen density.

3.1. Generation of a three-dimensional map of the $O_2(a^1\Delta)$ density

The excited O_2 density can directly be calculated from the following equation (see reaction 2):

$$[O_2{}^*](z) = \frac{\eta(z)}{A} \qquad 6$$

where $[O_2{}^*]$ is the molecular excited oxygen density expressed in cm^{-3} and A=2.19x10^{-4} s^{-1} is the Einstein coefficient of the 1.27 µm transition (Newman *et al.*, 1999). Applying this equation to every single point of the Venus nightside leads to the generation of a three-dimensional map of the molecular oxygen density. This leads to the conclusion that the mean altitude of the peak emission rate is located at 99.2 km, with a maximum value of 6.5x10^9 cm^{-3} and a mean weighted value at the peak of 2.1x10^9 cm^{-3}. The global morphology of the $O_2(a^1\Delta)$ density is similar to the maps presented in Figure 1.

3.2. Generation of a three-dimensional map of the CO_2 density

CO_2 density profiles have first been obtained from the VTS3 model. At a given altitude, the CO_2 densities predicted by VTS3 are equal for a fixed solar zenith angle. This can be explained because VIRA is based on PVO measurements, which only collected in situ measurements at low latitudes. To make up for the lack of data at higher latitudes when constructing the VTS3 model, the PVO observations were grouped depending on their distance to the antisolar point along the equator and circularized. The symmetrical distribution of the VTS3 CO_2 density is represented in black in Figure 4. The curve shapes are identical in both cases (at 97 and 105 km): the CO_2 density remains constant between 0° and 10° of antisolar angle, then decreases down to a minimum near 40° and finally increases to reach a maximum value near the terminator.

CO_2 profiles can also be retrieved from SPICAV stellar occultation observations (Figure 3), which have been acquired regardless of the VIRTIS observations. To infer the amount of CO_2 molecules along the line of sight, the stellar beam dimming of a bright UV star between 120 and 200 nm is measured outside and trough the Venusian atmosphere. The inversion routine of Montmessin *et al.* (2006a; 2006b) based on Quémerais *et al.* (2006) considers the Beer–Lambert's law, expressing that source attenuation scales exponentially with opacity. Spectral inversion is performed independently for every altitude with a least-squares fitting technique (Levenberg–Marquardt) to infer the number of CO_2 molecules and the aerosol opacity integrated over the line of sight. Based on the previous results from the VIRA model, the 114 SPICAV stellar occultation observations were grouped by steps of 15°, depending on their distances to the antisolar point. An averaged CO_2 density profile was finally generated for each group of profiles. Its associated solar zenith angle was calculated by averaging the distances associated to every single profile of the group. The full set of profiles is plotted in Figure 5 and the CO_2 densities at a given altitude are represented with diamonds in Figure 4.

Between 0° and 50°, the shapes of the SPICAV profiles are identical to those from the VTS3 model, with a minimum near 40°. By contrast, the SPICAV densities show a pronounced drop beyond 50°, which is the opposite of the VTS3 predictions. However, it is important to stress that VTS3 densities below 145 km high only are extrapolations of higher altitude measurements based on hydrostatic equilibrium. It is also important to note that the CO_2 densities obtained with SPICAV are always smaller than those of VTS3 at 97 km, while they are larger between 0° and 60° at 105 km.

3.3. Generation of a three-dimensional map of the atomic oxygen density

Finally, the oxygen density can be deduced from $O_2(a^1\Delta)$ and CO_2 densities (see reactions 1 to 3):

$$[O](z) = \sqrt{[O_2{*}](z)\frac{A + C_q[CO_2](z)}{k\varepsilon[CO_2](z)}} \qquad 7$$

where $[O]$ is the atomic oxygen density expressed in cm^{-3} and ε is the efficiency of the $a^1\Delta$ state production in reaction 1 assumed to be 75%. The local CO_2 density can be calculated for any point of Venus nightside either by using the VTS3 model with the appropriate coordinates (latitude and local time of the point) or by interpolating the six profiles obtained with the SPICAV measurements (given the zenithal distance of the point). The resulting three-dimensional map of the atomic oxygen density can be represented at a fixed altitude of 103 km, for instance, both for the calculation made with the VTS3 CO_2 densities (Figure 6-a) or the SPICAV CO_2 measurements (Figure 6-b). In both cases, the hemispheric area weighted mean O density at the peak is 2.0×10^{11} cm^{-3}. Using CO_2 densities from VTS3, the mean

altitude of the peak is located at 106.1 km while it is located at 103.4 km if CO_2 densities from SPICAV stellar occultations are used. The general morphology of the density maps also shows differences using one method or the other. For example, the maximum O density at 103 km reaches $3.4x10^{11}$ cm^{-3} near the antisolar point with the VTS3 CO_2 densities while it is $3.2x10^{11}$ cm^{-3} with the SPICAV CO_2 dataset. Instead, values obtained near the terminator are lower when using the VTS3 data: at 0400 LT and 30°S, the O densities are $1.0x10^{11}$ cm^{-3} and $1.2x10^{11}$ cm^{-3} for the CO_2 data from VTS3 and SPICAV, respectively. This can be explained considering Figure 4-b and equation 7. Near the terminator, CO_2 density values from VTS3 are higher than those derived from SPICAV observations and the O density is inversely proportional to the square root of the CO_2 density. Therefore, the O density calculated with CO_2 values derived from VTS3 are expected to be less than those calculated with the SPICAV CO_2 profiles. Finally, maps of Figure 6 shows that the higher O densities are located around the antisolar point for the densities calculated with CO_2 densities from SPICAV observations (Figure 6-b) while they are more scattered for the O densities deduced from VTS3 CO_2 simulations (Figure 6-a). Figure 6-c and Figure 6-d respectively represent cuts through the atmosphere along the equator and along the midnight meridian to illustrate the vertical distribution of the oxygen density. Once again, a brighter area appears near the antisolar point, especially between 101 and 106 km. Considering the distribution of a given density level, it is seen that the altitude of the layer increases away from the antisolar point. This is likely a consequence of the increase of the $O_2(a^1\Delta)$ intensity reference profiles away from the antisolar point (see Figure 2-b).

It is also interesting to compare these results to the O densities directly derived from the VTS3 model and which currently are the only ones available. Whatever the altitude, the atomic oxygen density in VTS3 is constant along any given solar zenithal distance, meaning that they are axi-symetric along the Sun-Venus axis (for the same reason as VTS3 CO_2

profiles are concentrically distributed), which can hardly reproduce the reality. At 103 km, the density variations follow the same shape as the plot of the VTS3 CO_2 density presented in black in Figure 4-b. The VTS3 O density at the antisolar point (0° of antisolar angle) is $5.8x10^{10}$ cm^{-3}, reaches $6.0x10^{10}$ cm^{-3} at 16°, decreases down to $5.2x10^{10}$ cm^{-3} at 38° and then increases continuously to reach $6.6x10^{10}$ cm^{-3} at the terminator. The mean value at 103 km is $6.4x10^{10}$ cm^{-3} which is about 3 times less than for the O density previously calculated with CO_2 densities from VTS3 and SPICAV. A comparison between the results obtained for the derivation of a density profile at 0045 LT and 24°S using either directly the VTS3 model (dotted line) or CO_2 densities from the VTS3 model (dashed line) or based on the $O_2(a^1\Delta)$ airglow profiles combined with CO_2 densities from the SPICAV stellar occultations (solid line) is shown in Figure 7. While the dashed and solid lines show a density peak near 105 km, the VTS3 model only simulates an exponential decrease of the O density with altitude. As already mentioned, this is because VTS3 below 145 km only is a downward extrapolation of the PVO measurements assuming hydrostatic equilibrium.

4. Discussion

This study provides a detailed description of the $O_2(a^1\Delta)$ emission and O density in the Venus nightside lower thermosphere and upper mesosphere. So far, only O density simulations from the VTS3 model, based on extrapolation of measurements collected by the Pioneer Venus mass spectrometer above 145 km were available. Is this study, we construct a three-dimensional map of the atomic oxygen density using observations by VIRTIS at 1.27 µm. It is based on the analysis of the $O_2(a^1\Delta)$ nightside emission and measurements of the CO_2 density with stellar occultations by SPICAV. Results obtained with this method appear more realistic than those obtained with the VTS3 model, especially given the morphology of the O density

distribution. The three-dimensional map of oxygen density has been generated using interesting intermediate tools. A complete three-dimensional statistical map of the $O_2(a^1\Delta)$ nightglow has been built with limb and nadir observations to obtain a coverage of Venus nightside both in the northern and in the southern hemispheres. A three-dimensional statistical map of the metastable molecular oxygen density has also been deduced. Finally, three-dimensional maps of the CO_2 density have been generated, either by using the VTS3 model or SPICAV stellar occultations. Comparison of these two sets of results shows that even if plots of the CO_2 densities as a function of the antisolar angle present the same shape at a given altitude (plateau around the antisolar point, minimum near 40°), important density differences are observed, especially near the terminator. Using these results, three-dimensional maps of the atomic oxygen density have been constructed. However, some uncertainties remain. For example, the quenching coefficient of $O_2(a^1\Delta)$ by CO_2 has never been measured and the value used in this study is an upper limit. A value of Cq=0 in equation 7 would lead to O densities 1.5% smaller than those obtained here. Similarly, O densities would have been 15% less if an efficiency of 100% had been used. Also, the k reaction rate for three-body recombination is estimated to be 2.5 times the value of the coefficient for oxygen atom three-body recombination in nitrogen but has not been measured with CO_2 as a third body.

The current results can be used as constraints to the composition of Venus nightside atmosphere predicted by such models. We note that recent model predictions are in good agreement with these results. The three-dimensional Venus Thermospheric General Circulation Model (Bougher *et al.,* 2010; Brecht *et al.,* 2010), which combines chemical, dynamical and energetic processes, calculates an oxygen density of 2.4×10^{11} cm^3 at 104 km. The one-dimensional photochemical model of Krasnopolsky (2010) for the Venus nightside, which involves 61 reactions and 24 species, predicts an O density profile of about 2×10^{11} cm^3 between 104 and 112 km. Future improved statistics of the SPICAV observations will

contribute to a better assessment of the distribution of CO_2 in the thermosphere-mesosphere transition region and thus, to the accuracy of the O distribution on the Venus nightside.

Acknowledgements

We gratefully thank all members of the ESA Venus Express project and of the VIRTIS and SPICAV scientific and technical teams. L. Soret was supported by the PRODEX program managed by the European Space Agency with the help of the Belgian Federal Space Science Policy Office. J.-C. Gérard acknowledges funding from the Belgian Fund for Scientific Research (FNRS). This work was funded by Agenzia Spaziale Italiana and the Centre National d'Etudes Spatiales.

Figure captions

Figure 1: Statistical map of the $O_2(a^1\Delta)$ nightglow in a nadir geometry view (a) generated with limb and nadir observations (b) and cross section at 96.5 km of the three-dimensional statistical map of the $O_2(a^1\Delta)$ nightglow.

Figure 2: Averaged limb brightness profiles according to their distance from the antisolar point deduced from limb observations in the northern hemisphere (a) and variation of the peak altitudes according to their distance to the antisolar point (b). The peak intensity tends to decrease while moving toward the pole while the peak altitude tends to increase.

Figure 3: SPICAV stellar occultations distribution over the Venus nightside.

Figure 4: Cross sections of CO_2 densities as a function of the distance to the antisolar point at 97 km (a) and 105 km (b). The CO_2 densities calculated with the VTS3 model are plotted in solid line while those derived from SPICAV stellar occultations are represented with diamonds.

Figure 5: Averaged CO_2 density profiles calculated from SPICAV observations between 80 and 140 km (a) and between 90 and 110 km (b).

Figure 6: Cross section at 103 km of the three-dimensional map of the atomic oxygen density generated with CO_2 density profiles from the VTS3 model (a) and from SPICAV measurements (b). Cross sections of the three-dimensional map of the atomic oxygen density generated with CO_2 density profiles from SPICAV measurements at the equator (c), using

averaged values between 5°S and 5°N. Cross sections of the three-dimensional map of the atomic oxygen density generated with CO_2 density profiles from SPICAV measurements along the midnight meridian (d), generated with averaged values between -0030 and +0030 LT. Black pixels mean that no data were available.

Figure 7: Comparison of the oxygen density profiles obtained with the VTS3 simulation (dotted line), the calculation with CO_2 densities from VTS3 (dotted line) and the calculation with CO_2 densities from SPICAV observations (solid line).

References

Bailey, J., Chamberlain, S., Crisp, D., Meadows, V. S., 2008. Near infrared imaging spectroscopy of Venus with the Anglo-Australian Telescope, Planet. Space Sci. 56, 1385-1390.

Bertaux, J.-L., et al., 2007. SPICAV on Venus Express: Three spectrometers to study the global structure and composition of the Venus atmosphere, Planet. Space Sci. 55, 1673-1700.

Bougher, S. W., Brecht, A., Parkinson, C. D., Rafkin, S., Gérard, J.-C., Yung, Y. L., 2010. Dynamics, Airglow, and Chemistry of the Venus Upper Atmosphere: Interpretation of Venus Express Datasets Using the VTGCM, International Venus Conference, Aussois, p. 94 (abstract).

Brecht, A., Bougher, S. W., Parkinson, C. D., Rafkin, S., Gérard, J.-C., 2010. Concurrent observations of the ultraviolet NO and infrared O_2 nightglow emissions: Uncorrelated behavior explained with the VTGCM, International Venus Conference, Aussois, p. 95 (abstract).

Cardesin-Moinelo, A., 2009. Studio ed implement azione della pipeline dei dati dello spettrometro ad immagini VIRTIS a bordo della mission Venus Express: "Dalla planificazione scientifica delle operazioni fino all'archiviazione dei dati ed all'elaborazione ad alto livello". Thesis, Università degli Studi di Padova, Italy, 207pp.

Connes, P., Noxon, J. F., Traub, W. A., Carleton, N. P., 1979. $O_2(^1\Delta)$ emission in the day and night airglow of Venus, Astrophys. J. 233, 29-32.

Cox, C., Saglam, A., Gérard, J. C., Bertaux, J. L., Gonzalez-Galindo, F., Leblanc, F., Reberac, A., 2008. Distribution of the ultraviolet nitric oxide Martian night airglow: Observations from Mars Express and comparisons with a one-dimensional model, J. Geophys. Res.-Planets 113.

Crisp, D., Meadows, V. S., Bezard, B., deBergh, C., Maillard, J. P., Mills, F. P., 1996. Ground-based near-infrared observations of the Venus nightside: 1.27 μm $O_2(a^1\Delta_g)$ airglow from the upper atmosphere, J. Geophys. Res.-Planets 101, 4577-4593.

Drossart, P., et al., 2007. Scientific goals for the observation of Venus by VIRTIS on ESA/Venus express mission, Planet. Space Sci. 55, 1653-1672.

Gérard, J. C., Saglam, A., Piccioni, G., Drossart, P., Cox, C., Erard, S., Hueso, R., Sanchez-Lavega, A., 2008. Distribution of the O_2 infrared nightglow observed with VIRTIS on board Venus Express, Geophys. Res. Lett. 35.

Gérard, J. C., Saglam, A., Piccioni, G., Drossart, P., Montmessin, F., Bertaux, J. L., 2009. Atomic oxygen distribution in the Venus mesosphere from observations of O_2 infrared airglow by VIRTIS-Venus Express, Icarus 199, 264-272.

Gérard, J. C., Soret, L., Saglam, A., Piccioni, G., Drossart, P., 2010. The distributions of the OH Meinel and $O_2(a^1\Delta\text{-}X^3\Sigma)$ nightglow emissions in the Venus mesosphere based on VIRTIS observations, Adv. Space Res. 45, 1268-1275.

Hedin, A. E., Niemann, H. B., Kasprzak, W. T., Seiff, A., 1983. Global Empirical Model of The Venus Thermosphere, J. Geophys. Res. 88, 73-83.

Huestis, D. L., Bougher, S. W., Fox, J. L., Galand, M., Johnson, R. E., Moses, J. I., Pickering, J. C., 2008. Cross Sections and Reaction Rates for Comparative Planetary Aeronomy, Space Sci. Rev. 139, 63-105.

Keating, G. M., Bertaux, J. L., Bougher, S. W., Dickinson, R. E., Cravens, T. E., Hedin, A. E., 1985. Venus international reference atmosphere, Adv. Space Res. 5, 117-171.

Krasnopolsky, V. A., 2010. Venus night airglow: Ground-based detection of OH, observations of O_2 emissions, and photochemical model, Icarus 207, 17-27.

Leu, M. T., Yung, Y. L., 1987. Determination of the $O_2(^1\Delta)$ and $O_2(^1\Sigma)$ yields in the reaction O + ClO = Cl + O_2: Implications for photochemistry in the atmosphere of Venus, Geophys. Res. Lett. 14, 949-952.

Montmessin, F., et al., 2006a. Subvisible CO_2 ice clouds detected in the mesosphere of Mars, Icarus 183, 403-410.

Montmessin, F., Quémerais, E., Bertaux, J. L., Korablev, O., Rannou, P., Lebonnois, S., 2006b. Stellar occultations at UV wavelengths by the SPICAM instrument: Retrieval and analysis of Martian haze profiles, J. Geophys. Res. 11.

Newman, S. M., Lane, I. C., Orr-Ewing, A. J., Newnham, D. A., Ballard, J., 1999. Integrated absorption intensity and Einstein coefficients for the O_2 $a^1\Delta_g$–$X^3\Sigma_g^-$ (0,0) transition: A comparison of cavity ringdown and high resolution Fourier transform spectroscopy with a long-path absorption cell, J. Chem. Phys. 110, 10749-10757.

Niemann, H. B., Kasprzak, W. T., Hedin, A. E., Hunten, D. M., Spencer, N. W., 1980. Mass Spectrometric Measurements of the Neutral Gas Composition of the Thermosphere and Exosphere of Venus, J. Geophys. Res. 85, 7817-7827.

Ohtsuki, S., Iwagami, N., Sagawa, H., Kasaba, Y., Ueno, M., Imamura, T., 2005. Ground-based observation of the Venus 1.27 μm O_2 airglow, in: Witasse, O., Shea, M. A. (Eds.), Planetary Atmospheres, Ionospheres, and Magnetospheres, pp. 2038-2042.

Ohtsuki, S., Iwagami, N., Sagawa, H., Ueno, M., Kasaba, Y., Imamura, T., Nishihara, E., 2008. Imaging spectroscopy of the Venus 1.27 μm O_2 airglow with ground-based telescopes, Adv. Space Res. 41, 1375-1380.

Piccioni, G., Zasova, L., Migliorini, A., Drossart, P., Shakun, A., Munoz, A. G., Mills, F. P., Cardesin-Moinelo, A., 2009. Near-IR oxygen nightglow observed by VIRTIS in the Venus upper atmosphere, J. Geophys. Res.-Planets 114.

Quémerais, E., Bertaux, J. L., Korablev, O., Dimarellis, E., Cot, C., Sandel, B. R., Fussen, D., 2006. Stellar occultations observed by SPICAM on Mars Express, J. Geophys. Res. 111.

Sander, S. P., et al., 2003. Chemical Kinetics and Photochemical Data for Use in Atmospheric Studies, JPL publication 02-25.

Slanger, T. G., Huestis, D. L., Cosby, P. C., Chanover, N. J., Bida, T. A., 2006. The Venus nightglow: Ground-based observations and chemical mechanisms, Icarus 182, 1-9.

Figures

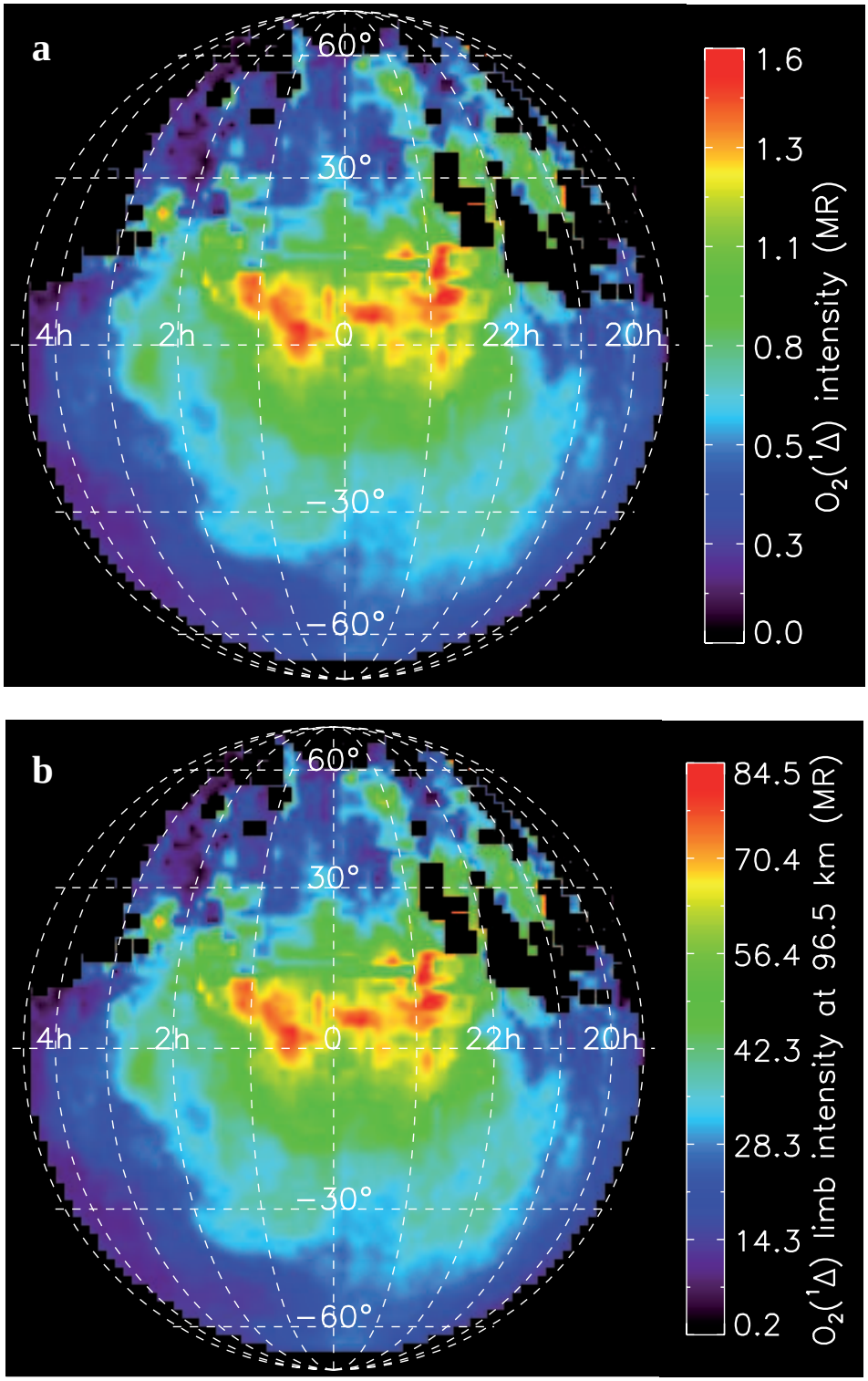

Figure 1

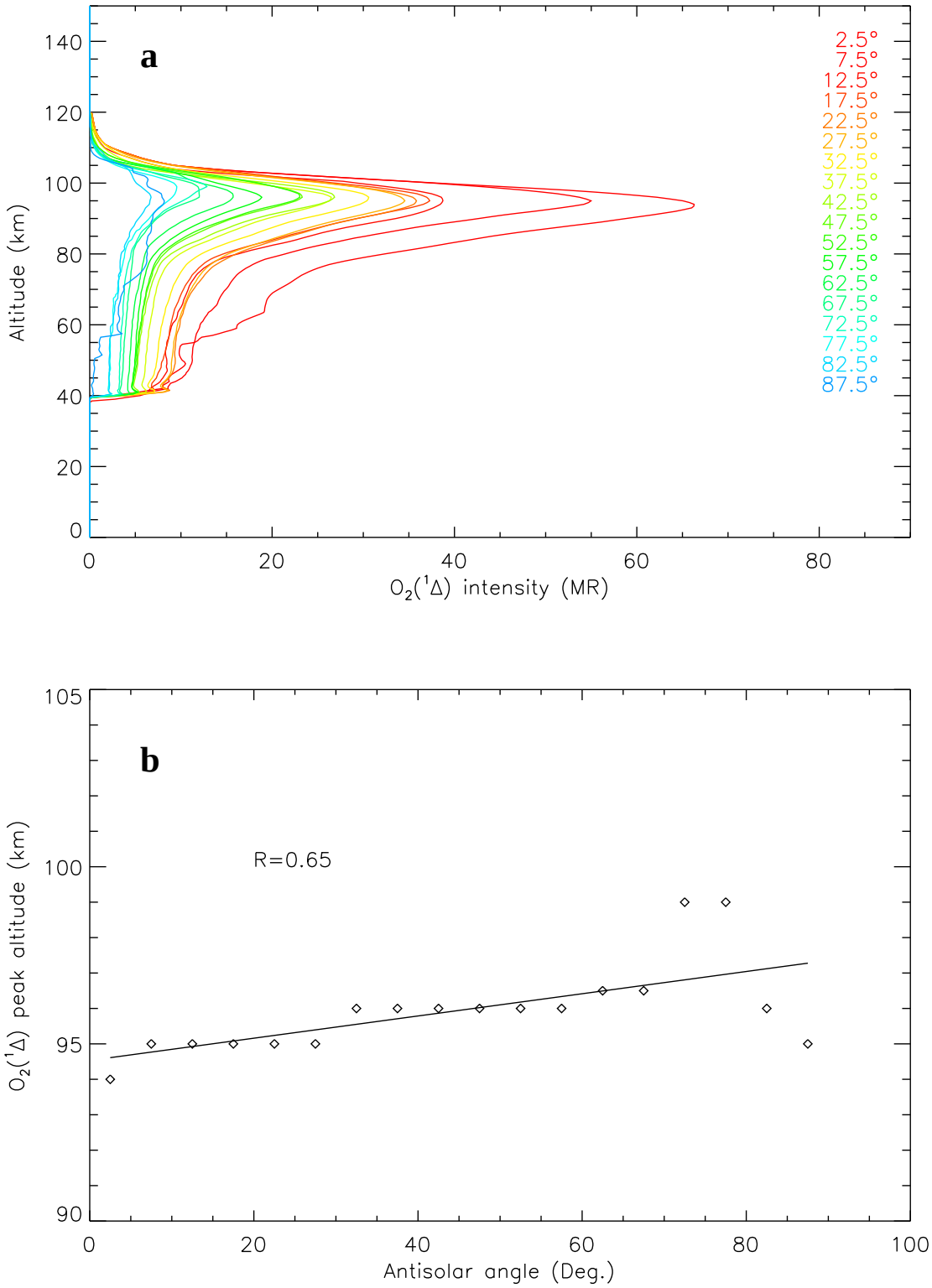

Figure 2 (a and b)

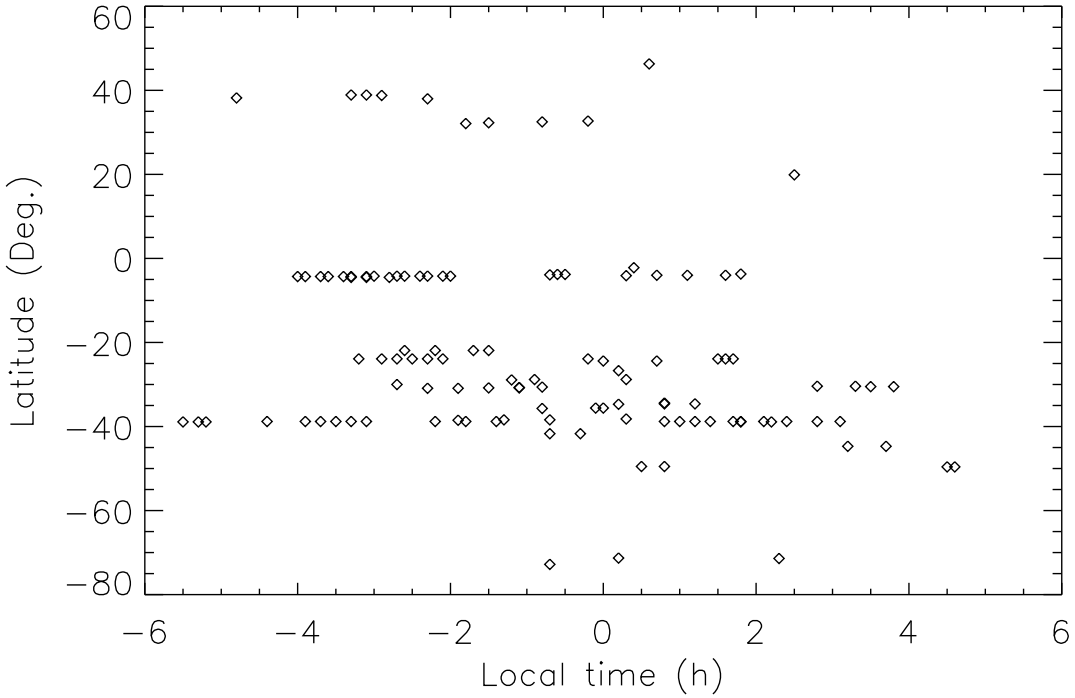

Figure 3

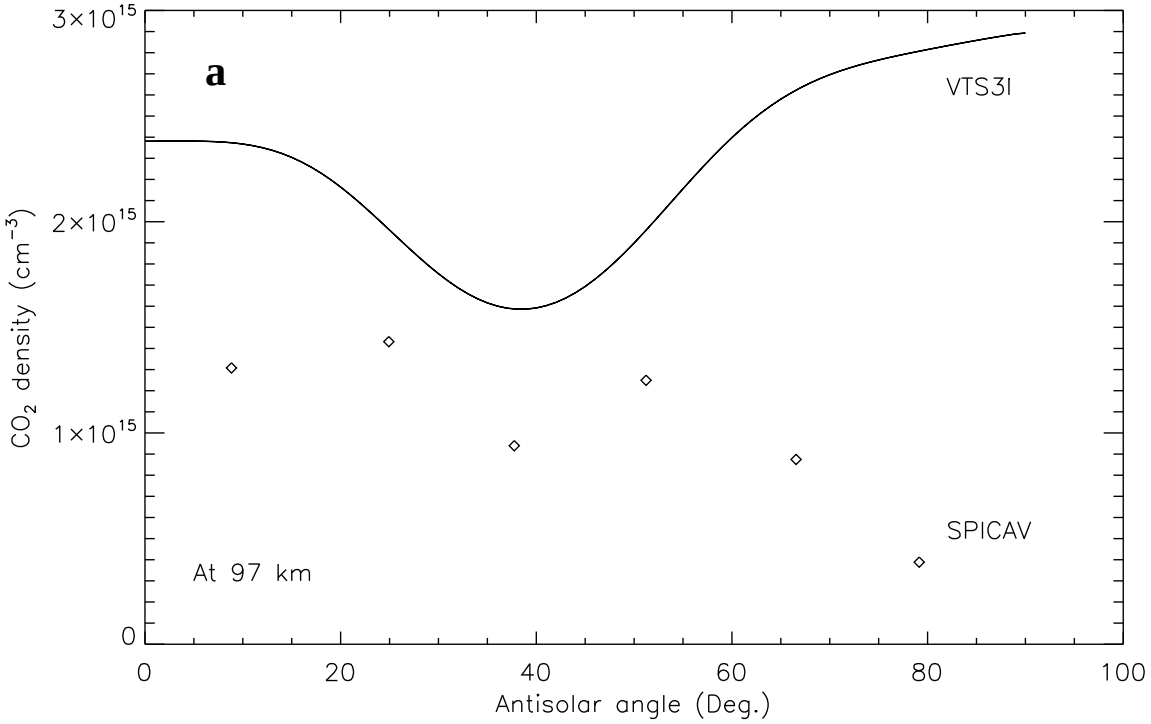

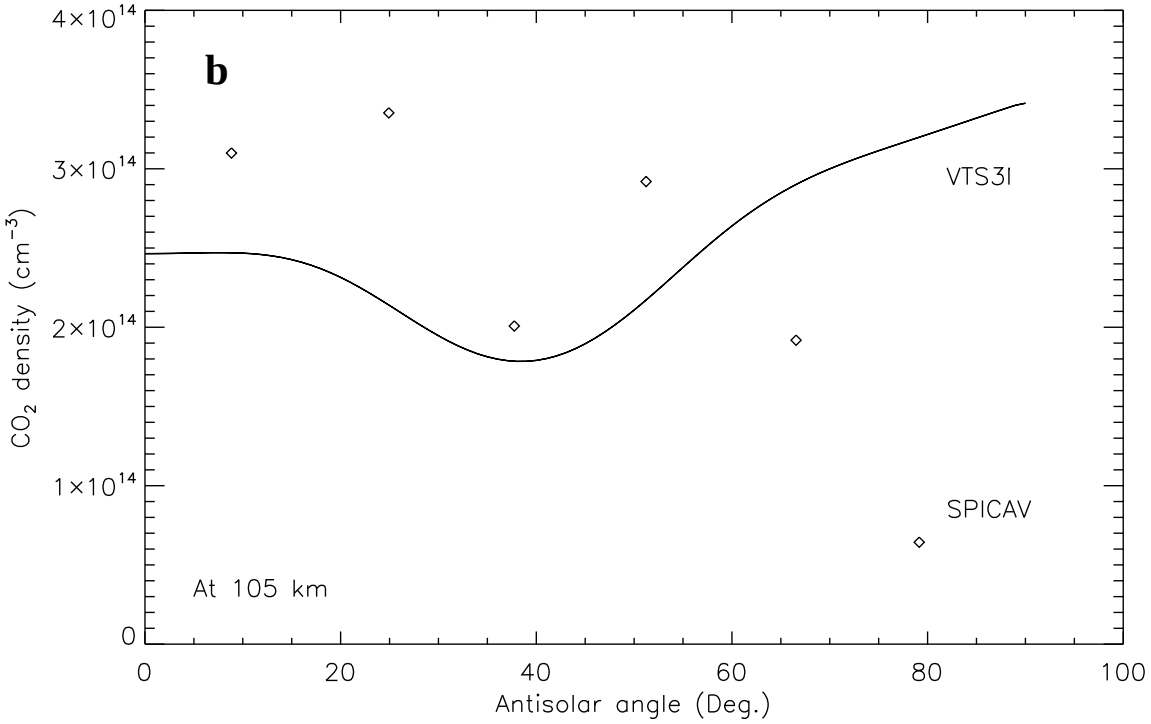

Figure 4: (a and b)

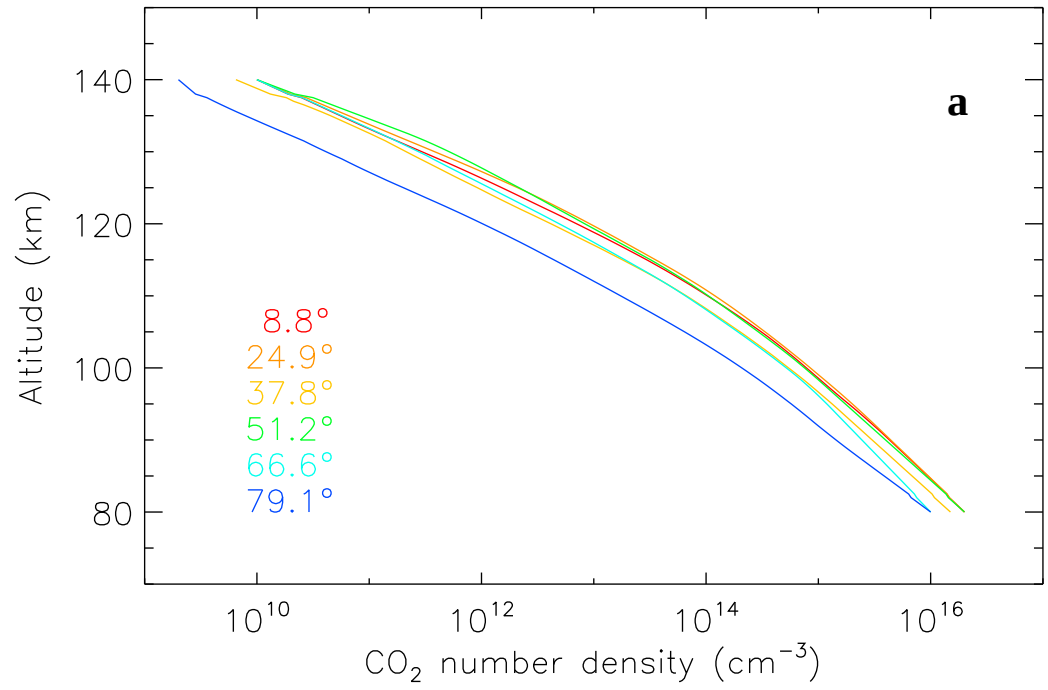

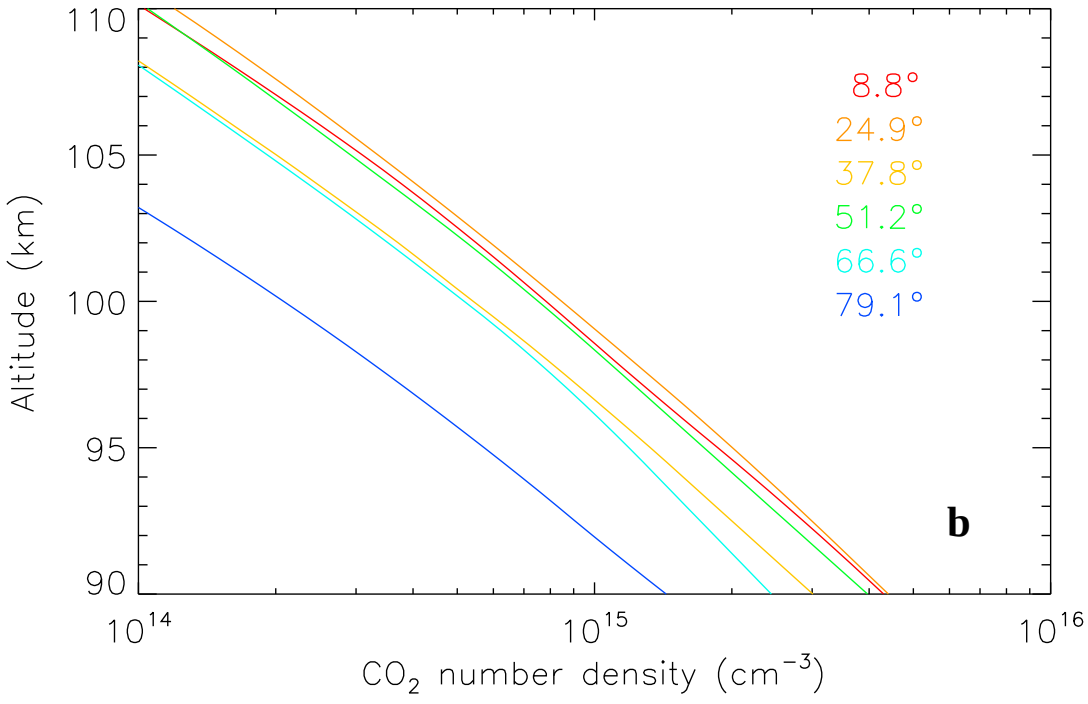

Figure 5 (a and b)

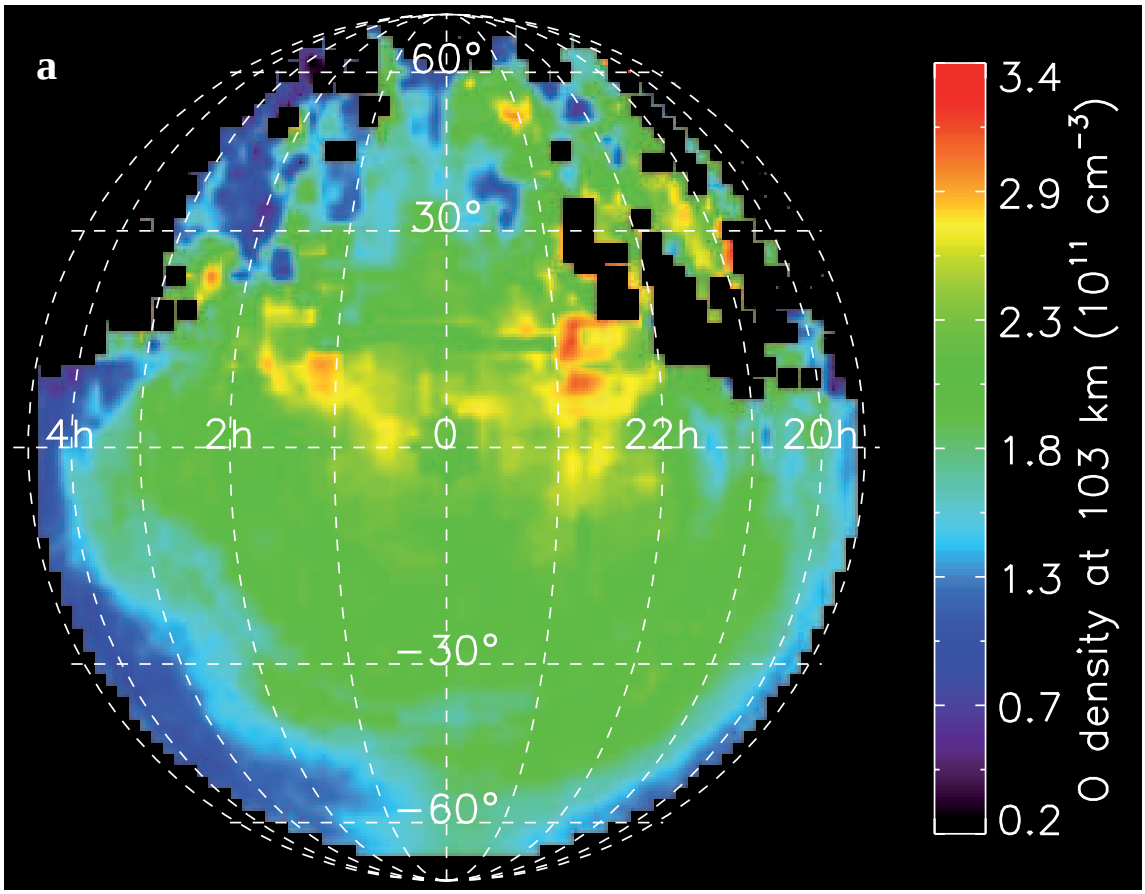
a
60°
30°
4h
2h
0
22h
20h
−30°
−60°
3.4
2.9
2.3
1.8
1.3
0.7
0.2
O density at 103 km (10^11 cm^-3)

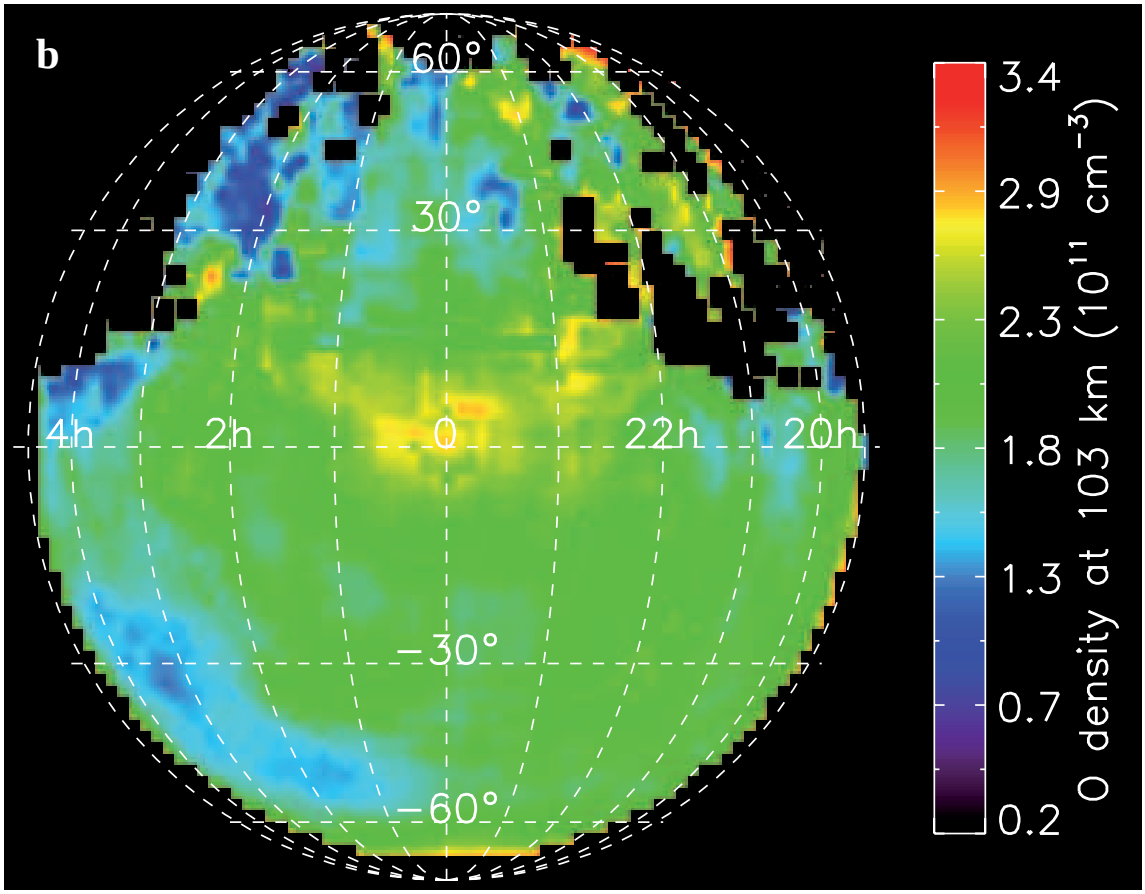
b
60°
30°
4h
2h
0
22h
20h
−30°
−60°
3.4
2.9
2.3
1.8
1.3
0.7
0.2
O density at 103 km (10^11 cm^-3)

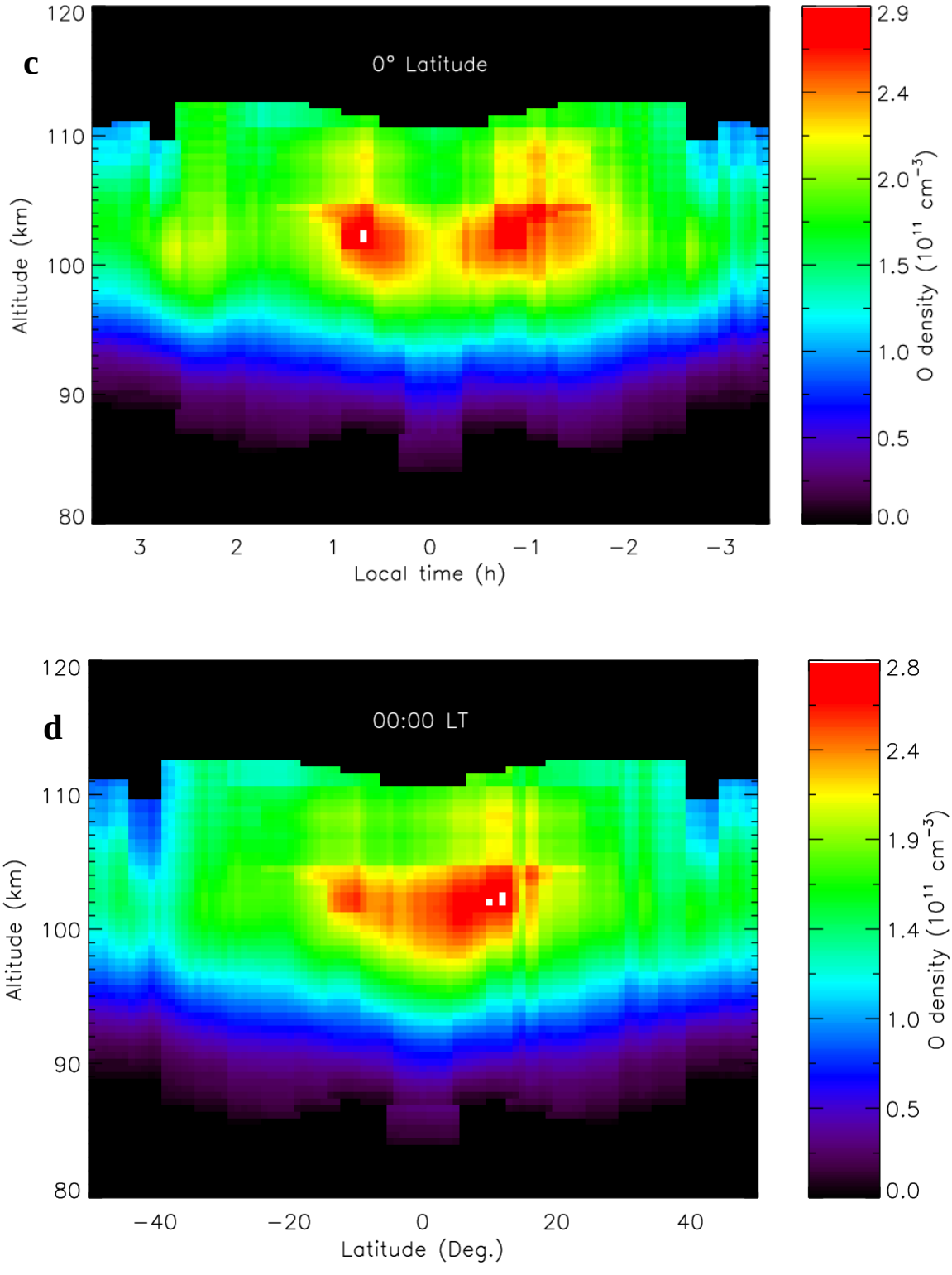

Figure 6 (a, b, c and d)

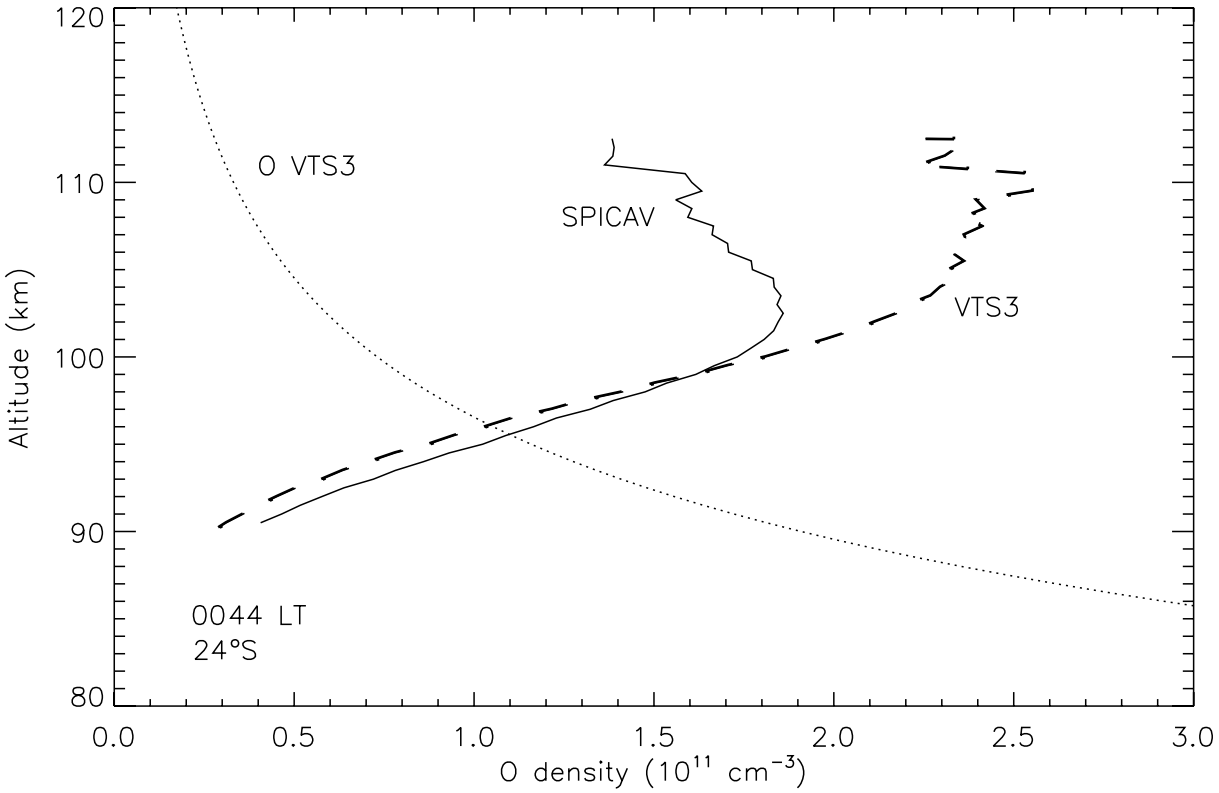
120
110
100
90
80
Altitude (km)
O VTS3
SPICAV
VTS3
0044 LT
24°S
0.0
0.5
1.0
1.5
2.0
2.5
3.0
O density (10^{11} cm^{-3})

Figure 7